Theory of nanolaser devices: Rate equation analysis versus microscopic theory

Lorke, Michael; Skovgård, Troels Suhr; Gregersen, Niels; Mørk, Jesper

Published in:
Physical Review B (Condensed Matter and Materials Physics)

Link to article, DOI:
10.1103/PhysRevB.87.205310

Publication date:
2013

Document Version
Publisher's PDF, also known as Version of record

Theory of nanolaser devices: Rate equation analysis versus microscopic theory

M. Lorke,* T. Suhr, N. Gregersen, and J. Mørk

DTU Fotonik, Department of Photonics Engineering, and Technical University of Denmark, Building 343, 2800 Kgs. Lyngby, Denmark

(Received 25 July 2012; revised manuscript received 25 March 2013; published 28 May 2013)

A rate equation theory for quantum-dot-based nanolaser devices is developed. We show that these rate equations are capable of reproducing results of a microscopic semiconductor theory, making them an appropriate starting point for complex device simulations of nanolasers. The input-output characteristics and the modulation response are investigated and the limits of the rate equation approach are discussed.

DOI: 10.1103/PhysRevB.87.205310 PACS number(s): 78.67.Hc, 78.45.+h, 42.30.Lr

I. INTRODUCTION

In the emerging field of photonic signal processing there is an expressed need for small and efficient light emitters that can be integrated in photonic circuits. Semiconductor lasers are central to a number of optical technologies. They are most prominently used in optical communications and optical data storage involving compact disks, digital versatile disks, and Blu-ray disks. Recently, semiconductor active regions coupled with nanoscale optical resonator schemes, such as micropillar or photonic-crystal cavities, have opened an additional level of miniaturization and facilitated the implementation of photonic integrated circuits. In the past two decades process technology has matured sufficiently to enable fabrication of active cavities with high quality factors and low mode volumes,[1] where the Purcell enhancement of spontaneous emission[2] can become large enough to affect the dynamics of the device. For practical applications, semiconductor quantum dots (QDs) have proven to be an interesting system, as they possess a discrete energy spectrum that can be engineered to a large extent. They are considered as gain material for next generation optoelectronic devices and for fundamental studies of light-matter interaction.[3–5] The advent of photonic crystals allows one to combine QDs with high-quality cavities,[6–9] which opens a multitude of possibilities for guiding and modifying the emission properties of QD-based devices via Purcell enhancement of emission rates.[9] Therefore, the laser dynamics of nanocavity-based laser devices has been a much debated topic in recent years (see, e.g., Refs. 10–16).

Early predictions of the properties of nanolasers by Altug *et al.*[17] were based on an analysis of the laser rate equations with a phenomenological Purcell enhancement of the spontaneous emission rate. While most studies of the input-output characteristics are based on phenomenological rate equation approaches, microscopic theories have also been developed.[18] These theoretical models have been used in the past to study the emission properties of QD-based microcavity lasers[18–20] as well as correlation functions such as $g^{(2)}(0)$,[19,21] that contain information about the coherence properties of the emitted light. Several of these works included comparisons to experiment, that showed good agreement of the microscopic model with experimental data and we therefore choose the microscopic model as a benchmark for the rate equation theory. The correct way to implement Purcell enhancement into the rate equations seems unclear in the literature. Early work[22–24] accounted for the cavity induced enhancement of the spontaneous emission rate, as originally suggested by Purcell, but also included enhancement of the stimulated emission rate, motivated by the Einstein relation between these rates. Experimental evidence for Purcell enhancement of stimulated emission was presented in Refs. 25 and 26. In recent work, however, only the rate of spontaneous emission was considered to be Purcell enhanced,[12,17] neglecting the influence of Purcell enhancement on stimulated emission, which violates the Einstein relations and is problematic from a microscopic viewpoint, as we will see in what follows. Employing such a rate equation model for fitting experimental data will lead to a wrong estimation of parameters, e.g., the threshold, β factor, and modulation bandwidth. The intention of this paper is to clarify this situation by bridging the gap between a purely microscopic approach and a rate equation model that is suited for implementation in large-scale device simulations. We thus present the detailed derivation of our recently published rate equation model,[16] which naturally extends our previous models valid in the LED regime of spontaneous emission,[14,16] to account for spontaneous and stimulated emission rates in a self-consistent way.

The paper is structured as follows: In Sec. II A we describe the microscopic theory used as a benchmark for the rate equation model presented in Sec. II B. In Secs. III A and III B the rate equation approach and the microscopic theory are compared in terms of their predictions for the steady-state behavior as well as the modulation response.

II. THEORY

A. Microscopic description

We consider an ensemble of InGaAs QDs embedded in an optical nanocavity and take into account the two lowest confined shells for electrons and holes, that due to their angular momentum properties are labeled s- and p-shell, respectively. The optical mode is assumed to be on resonance with the s shells of the QDs, and for computational simplicity we neglect inhomogeneous broadening in the microscopic model. The QD s shells act as the laser levels, while a continuous wave pump is applied to the p shells. To study the dynamics of a nanocavity with a high enhancement of spontaneous emission, and for comparisons of nanoLEDs with nanolasers, we rely on a fully quantized description of the photon field.[18,21] Within the cluster expansion scheme, we derive equations of motion for the photon number in the mode q, $\langle b_q^\dagger b_q \rangle$

$$\left(\hbar\frac{d}{dt} + 2\kappa_q\right)\langle b_q^\dagger b_q\rangle = +2\,\mathrm{Re}\sum_{\nu'}|g_{q\nu'}|^2\langle b_q^\dagger v_{\nu'}^\dagger c_{\nu'}\rangle, \quad (1)$$

and the electron and hole population of the state ν, $f_\nu^{e,h}$

$$\hbar\frac{d}{dt}\,f_\nu^{e,h}\Big|_{\text{opt}} = -2\,\text{Re}\sum_q |g_{q\nu}|^2\langle b_q^\dagger v_\nu^\dagger c_\nu\rangle + S_\nu^{e,h} + \left(1-f_\nu^e-f_\nu^h\right)P_\nu. \tag{2}$$

Here $\kappa_q/\hbar$ is the inverse photon lifetime, giving the quality factor Q, P_ν is the pump excitation at the state ν, and

$$S_s^{e,h} = \left(1-f_s^{e,h}\right) f_p^{e,h}\, s^{e,h} \tag{3}$$

denotes population changes due to carrier scattering. We will treat the scattering rate $s^{e,h}$ as a free parameter in this work. Microscopically, it has contributions from Coulomb interaction[13,27] and carrier-LO-phonon interaction.[28,29] We only consider the scattering from the p shell to the s shell, which has proven to be a good approximation under laser conditions.

Both $\langle b_q^\dagger b_q\rangle$ and $f_\nu^{e,h}$ couple to the photon assisted polarization $\langle b_q^\dagger v_\nu^\dagger c_\nu\rangle$,[18]

$$\left(\hbar\frac{d}{dt}+\kappa_q+\gamma+i\left(\tilde\varepsilon_\nu^e+\tilde\varepsilon_\nu^h-\hbar\omega_q\right)\right)\langle b_q^\dagger v_\nu^\dagger c_\nu\rangle = f_\nu^e f_\nu^h - \left(1-f_\nu^e-f_\nu^h\right)\langle b_q^\dagger b_q\rangle + \delta\langle b_q^\dagger b_q c_\nu^\dagger c_\nu\rangle - \delta\langle b_q^\dagger b_q v_\nu^\dagger v_\nu\rangle, \tag{4}$$

where γ is an effective dephasing rate and $\tilde\varepsilon_\nu^{e,h}$ are the electron and hole energies of the QD s shell. The free evolution of $\langle b_q^\dagger v_\nu^\dagger c_\nu\rangle$ is determined by the detuning of the QD transitions from the cavity resonances $\hbar\omega_q$. In a semiconductor, the source term of spontaneous emission is described by the expectation value of four carrier operators $\langle c_\alpha^\dagger v_\alpha v_\nu^\dagger c_\nu\rangle$ (see Ref. 30). For uncorrelated carriers, the Hartree-Fock factorization of this source term leads to $f_\nu^e f_\nu^h$, which appears as the first term on the right-hand side of Eq. (4).

It should be noted here, that in the microscopic theory, both spontaneous and stimulated emission appear Purcell enhanced, since both are proportional to the light-matter coupling constant in Eq. (1) via the photon assisted polarization in Eq. (4). The coupling constant includes the Purcell enhancement via the vacuum field strength.

The higher correlation functions, $\delta\langle b_q^\dagger b_q c_\nu^\dagger c_\nu\rangle$ and $\delta\langle b_q^\dagger b_q v_\nu^\dagger v_\nu\rangle$ obey the equations of motion,[18]

$$\left(\hbar\frac{d}{dt}+2\kappa_q\right)\delta\langle b_q^\dagger b_q c_\nu^\dagger c_\nu\rangle = -2|g_{q\nu}|^2\text{Re}\left[\delta\langle b_q^\dagger b_q^\dagger b_q v_\nu^\dagger c_\nu\rangle + \left(\langle b_q^\dagger b_q\rangle + f_\nu^e\right)\langle b_q^\dagger v_\nu^\dagger c_\nu\rangle\right], \tag{5}$$

$$\left(\hbar\frac{d}{dt}+2\kappa_q\right)\delta\langle b_q^\dagger b_q v_\nu^\dagger v_\nu\rangle = +2|g_{q\nu}|^2\text{Re}\left[\delta\langle b_q^\dagger b_q^\dagger b_q v_\nu^\dagger c_\nu\rangle + \left(\langle b_q^\dagger b_q\rangle + f_\nu^h\right)\langle b_q^\dagger v_\nu^\dagger c_\nu\rangle\right]. \tag{6}$$

In this equation a quadruplet function enters, which represents a correlation between the photon-assisted polarization and the photon number. For the corresponding equation of motion we obtain

$$\left(\hbar\frac{d}{dt}+3\kappa_q+\gamma+i\left(\tilde\varepsilon_\nu^e+\tilde\varepsilon_\nu^h-\hbar\omega_q\right)\right)\delta\langle b_q^\dagger b_q^\dagger b_q b_q v_\nu^\dagger c_\nu\rangle = -2|g_{q\nu}|^2\langle b_q^\dagger v_\nu^\dagger c_\nu\rangle^2 - \left(1-f_\nu^e-f_\nu^h\right)\delta\langle b_q^\dagger b_q^\dagger b_q b_q\rangle + 2f_\nu^h\delta\langle b_q^\dagger b_q c_\nu^\dagger c_\nu\rangle - 2f_\nu^e\delta\langle b_q^\dagger b_q v_\nu^\dagger v_\nu\rangle + 2\langle b_q^\dagger b_q\rangle\left(\delta\langle b_q^\dagger b_q c_\nu^\dagger c_\nu\rangle - \delta\langle b_q^\dagger b_q v_\nu^\dagger v_\nu\rangle\right), \tag{7}$$

that couples to yet another correlation function, whose equation of motion is

$$\left(\hbar\frac{d}{dt}+4\kappa_q\right)\delta\langle b_q^\dagger b_q^\dagger b_q b_q\rangle = 4\sum_{\nu'}|g_{q\nu'}|^2\,\delta\langle b_q^\dagger b_q^\dagger b_q v_{\nu'}^\dagger c_{\nu'}\rangle. \tag{8}$$

It should be noted, that the latter is closely related to the intensity correlation function $g^{(2)}(\tau=0)$ via

$$g_q^{(2)}(\tau=0) = \frac{\langle n_q^2\rangle - \langle n_q\rangle}{\langle n_q\rangle^2} = 2 + \frac{\delta\langle b_q^\dagger b_q^\dagger b_q b_q\rangle}{\langle b_q^\dagger b_q\rangle^2}. \tag{9}$$

To derive a rate equation model, an adiabatic elimination of the photon assisted polarization has to be performed. From the formal solution of Eq. (4), it can easily be seen that an adiabatic elimination of the photon assisted polarization corresponds to a Markov approximation, i.e., the neglect of memory effects in $\langle b_q^\dagger v_\nu^\dagger c_\nu\rangle$. As the Markov approximation is trivially correct in steady state, a rate equation model should be able to capture the most relevant physics for these conditions.

B. Rate equations

For many applications and for inclusion in full-scale device simulation a rate-equation (RE) formulation that captures the essential features of the microscopic theory is advantageous. While there have been formulations of REs for nanocavity devices (see, e.g., Refs. 12 and 15–17) there is some confusion in the literature about the correct implementation of Purcell enhancement. In this work we bridge this gap by establishing a correct RE model that fits the results of the microscopic theory.

We start by defining the reduced electronic density of states (eDOS) for the combined system of N_{QD} quantum dots of total volume V_{QD} and including the continuum of wetting layer states,

$$\rho_r(E_{21}) = \frac{2N_{\text{QD}}}{V_{\text{QD}}\sqrt{2\pi\sigma^2}}e^{\frac{(E_s-E_{21})^2}{2\sigma^2}} + \frac{m_r}{\hbar^2\pi W}\Theta(E_{21}-E_{\text{WL}}). \tag{10}$$

Here, E_s is the transition energy of the s shell, V_{QD} is the QD volume, m_r is the reduced effective mass, W and E_{WL} are the wetting layer width and transition energy, and Θ is the Heaviside function. The factor of 2 takes into account the two electron spins. Included is additionally the inhomogeneous broadening σ, due to composition and size fluctuations of the QDs.

In Appendix A a general expression for the local density of states (LDOS) is given. In the following calculations, we employ a cavity LDOS, ρ_c, of the cavity mode at energy $\hbar\omega_c$, with linewidth $\delta\omega_c = \omega_c/Q$ and with Purcell factor F_p given

by

$$\rho_c(\hbar\omega') = \frac{F_p}{B_{21}\hbar\omega\tau_{21}} \frac{(\delta\omega_c)^2}{4(\omega-\omega_c)^2+(\delta\omega_c)^2}, \quad (11)$$

at a field antinode. Here the differential recombination lifetime τ_{21} is chosen such that the bulk spontaneous emission time τ_{hom} is recovered in the absence of a cavity.[14] The intrinsic Purcell factor is defined as $F_p = \frac{3Q}{4\pi^2 V}$ with the mode volume V given in units of $(\lambda/n)^3$, where n is the refractive index. The Purcell factor simply describes the increased LDOS at the resonance frequency, and it should not be mistaken for the Purcell enhancement describing the total emission rate into the cavity. This rate depends not only on the Purcell factor but also the details of the electronic DOS.[14]

Using these definitions, we can write the laser REs for the photon number n_p and the total excited carrier number n_{tot} as

$$\dot{n}_{\text{tot}} = P - r_c - r_b - r_{st}, \quad (12)$$

$$\dot{n}_p = r_c + r_{st} - \frac{n_p}{\tau_p}, \quad (13)$$

where P is the pump current and $\tau_p = (\delta\omega_c)^{-1}$ is the photon lifetime. Here, the rates of spontaneous r_c and stimulated r_{st} emission into the laser mode are

$$r_c = \int \rho_c(\hat{\mathbf{d}},\mathbf{r},\omega')\hbar\omega' B_{21}\rho_r(\mathbf{r},E_{21}) \times f_v(1-f_c)L(E_{21}-\hbar\omega')d\mathbf{r}dE_{21}\hbar d\omega', \quad (14)$$

$$r_{st} = n_p \int \rho_c(\hat{\mathbf{d}},\mathbf{r},\omega')\hbar\omega' B_{21}\rho_r(\mathbf{r},E_{21}) \times (f_c-f_v)L(E_{21}-\hbar\omega')d\mathbf{r}dE_{21}\hbar d\omega'. \quad (15)$$

In these equations, f_v and f_c are quasi-Fermi functions for the valence and conduction bands, respectively. The homogeneous broadening γ, which is caused at high carrier densities by excitation induced dephasing,[31] is taken into account with the introduction of the Lorentzian function L having linewidth γ.

The background emission rate r_b can be obtained by replacing the LDOS ρ_c in Eq. (14) with a background LDOS ρ_b. However, in the subsequent calculations we instead employ a background rate given by

$$r_b = r_c\left(\frac{1}{\beta}-1\right). \quad (16)$$

This definition of r_b is used so that the basic definition of the β factor,

$$\beta = \frac{r_c}{r_c+r_b}, \quad (17)$$

is observed. The definition (16) for the background emission is necessary for subsequent comparison with our microscopic model which requires a fixed β, i.e., independent of the carrier number. In Appendix A we present the general procedure for computing the β factor.

The total carrier density is found by evaluating

$$n_{\text{tot}} = \int \rho_r(\mathbf{r},E_{21})f_2(E_{21})L(\hbar\omega'-E_{21})\hbar d\omega' dE_{21}d\mathbf{r}, \quad (18)$$

and we assume that the electron and hole populations in the QDs are identical such that $f_2(E_s) = 1 - f_1(E_s)$. In these REs, not only *spontaneous* emission but also *stimulated* emission is Purcell enhanced. This can be seen as ρ_c appears both in r_c and r_{st}.

The basic limitations of the RE formalisms are, that they only work if the adiabatic elimination in Eq. (4) is appropriate, which is the case if the system is not in the strong coupling regime. Moreover, by determining the QD carrier populations using Eq. (18), we fix the carrier populations to be Fermi functions and therefore assume infinitely fast carrier scattering. While not being an intrinsic limitation, this assumption limits the applicability of the RE models for the analysis of dynamical quantities like the modulation response. However, as the modulation response is a small-signal quantity, the REs are applicable if the predicted modulation bandwidth does not exceed the inverse of the characteristic time of the scattering process that was neglected.

TABLE I. Parameters used in the calculations.

Parameter	Device A	Device B
Q	10 000	10 000
Purcell factor F_p	25	50
Homogeneous broadening (γ)	100 μeV	100 μeV
Number of QDs (N_{QD})	100	100
β factor	0.3	0.1
QD volume (V_{QD})	4000 nm^3	4000 nm^3

III. RESULTS

In this section we will compare the results of the microscopic theory to those of the modified REs presented in the preceding section. For the comparison we will employ two model devices labeled device A and device B. The parameters can be found in Table I. We will start by comparing steady-state results, that is, input-output characteristics. For the comparisons inhomogeneous broadening has been neglected for simplicity. The pump rates are scaled such that rates of carrier generation are the same in the two models.

A. Steady-state results

Figure 1 shows the input-output characteristics for device A with parameters according to Table I. The kink at the laser threshold in the input-output characteristics is clearly visible, although it should be emphasized that unlike in atomic rate equations, the height of the kink is *not* a direct measure of the β factor.[18] The modified rate equations agree well with the microscopic theory with the exemption of extremely high pump rate, where additional saturation of the pump levels leads to a different behavior of the microscopic theory. Also it should be noted that the influence of carrier-photon correlations, Eqs. (5)–(8), is negligible for the input-output characteristics for these parameters. Were we to model these I/O curves using an RE model without Purcell enhancement in the stimulated emission, a much higher optical gain, thus a higher number of QDs and a higher Q factor would be needed to reach the lasing regime. This accentuates the need to include Purcell enhancement in the model to correctly infer the parameters from comparisons between theory and experiment.

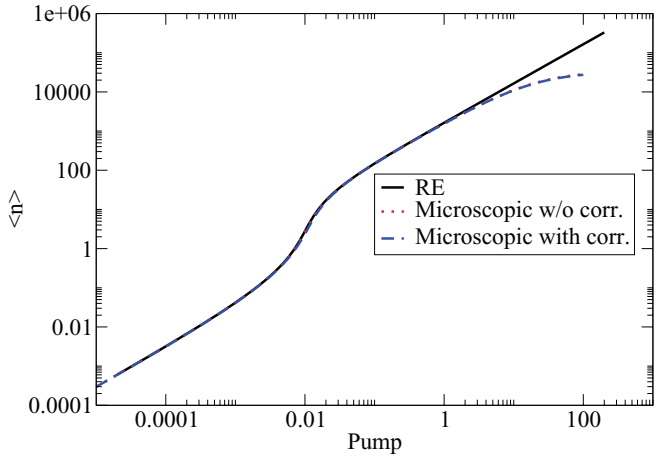

FIG. 1. (Color online) Input-output curve for device A. The RE theory (solid) is compared to the microscopic model with (dashed) and without (dotted) the inclusion of correlations according to Eqs. (5)–(8).

We want to point out that the connection between F_p and β is more complicated than in conventional edge emitting or VCSEL semiconductor devices and cannot be estimated by the simple expression $\beta = \frac{F_p}{F_p+1}$, but rather is given by

$$\beta = \frac{F_p}{F_p + \frac{R_{\rm nl}}{R_{\rm hom}}}. \tag{19}$$

Here, $R_{\rm hom}$ and $R_{\rm nl}$ are the emission rates into the homogeneous medium and into the nonlasing modes, respectively. For details see the article by J.-M. Gérard in Ref. 32. The connection between the β factor and the Purcell factor is more involved as some of the nonlasing modes, which lower the β factor, may be cavity modes of the same nanocavity as the laser mode. Therefore, they will possess the same low mode volume and the emission rate into these nonlasing modes will also be "Purcell enhanced," which lowers the β factor.

In Fig. 2 the comparison between RE analysis and microscopic theory is presented for device B. The conclusions are

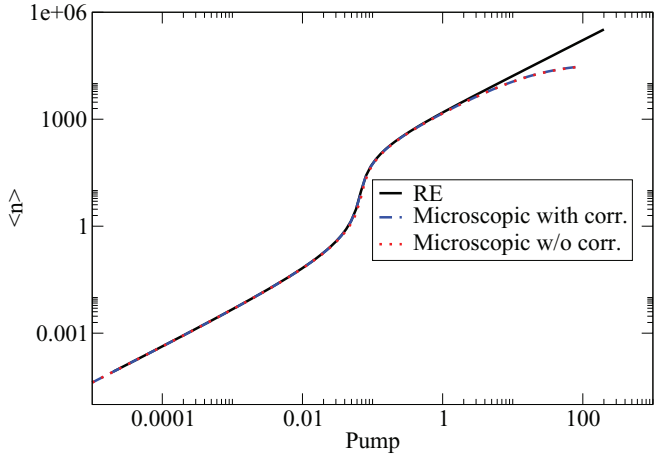

FIG. 2. (Color online) Input-output curve for device B. The RE theory (solid) is compared to the microscopic model with (dashed) and without (dotted) the inclusion of correlations according to Eqs. (5)–(8).

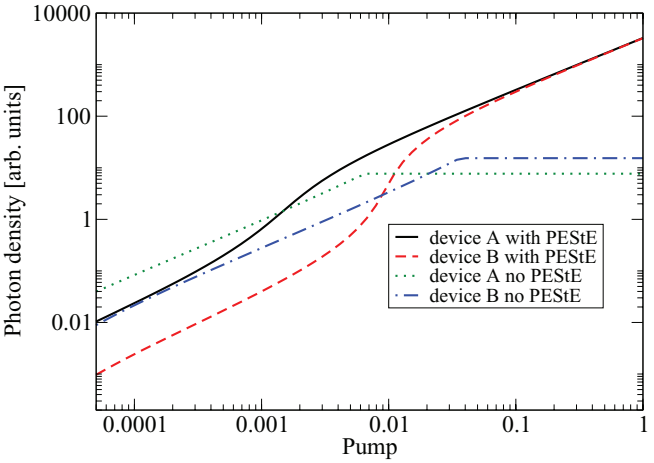

FIG. 3. (Color online) Input-output curves for the RE model with and without Purcell enhancement of the stimulated emission.

similar, the two theoretical models agree extremely well up to high pump rates, where deviations due to saturation effects occur. This suggests that our modified RE scheme is well versed to reproduce the essential features of the microscopic model and thus of the experiment. The advantage of the RE scheme is the ease with which arbitrary optical and electronic DOS can be incorporated in the model, which represents a major computational challenge for the microscopic model.

To demonstrate the importance of Purcell-enhanced stimulated emission (PEStE), model calculations with and without PEStE are presented in Fig. 3 in the framework of the RE model.[16] For both devices considered, the lasing threshold is not reached using the parameters employed in the microscopic theory. Here, we consider only the cavity contribution to light emission and not the background contribution R_b. Below threshold, the systems including PEStE also experience cavity enhanced absorption, and for a weak pump the photon numbers are thus lower than in the absence of PEStE. However, in the absence of PEStE the gain provided by the QD ensemble is insufficient to obtain lasing. The flattening of the curves do not indicate a threshold but simply a saturation of the photon number as the Fermi energy moves past the QD transition linewidth and starts feeding the wetting layer. We thus conclude that proper inclusion of Purcell enhancement is necessary to correctly predict parameters of the laser like, e.g., the threshold or material gain in nanocavity devices.

B. Modulation response

To use nanolasers in high-speed data communication applications, it is mandatory that they not only possess a beneficial input-output characteristic with low threshold current and high quantum efficiency, but also a high modulation bandwidth, as this is a key quantity for the realization of high-speed data communication applications. Therefore, we will investigate the modulation response of the two devices studied in the last section. The modulation response is evaluated by probing the system in steady state with a weak ultrashort test pulse. The modulation response function $h(\omega) = H(\omega)/H(0)$ is defined from the Fourier transform $H(\omega)$ of the response to the test pulse. As discussed in Sec. II B, the assumption of

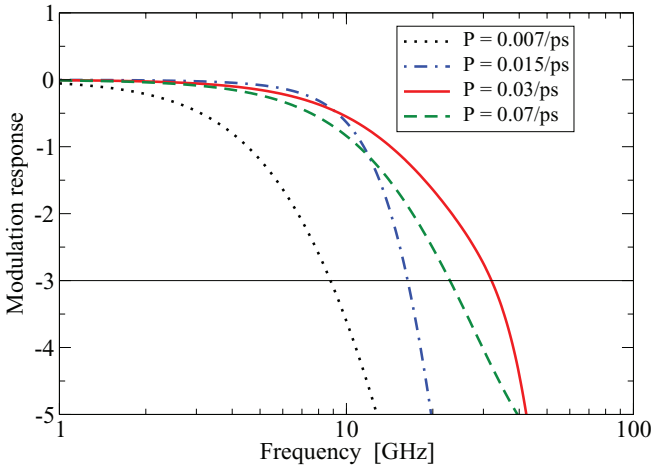

FIG. 4. (Color online) Modulation response for device A at various pump rates, as calculated from the microscopic model.

instantaneous carrier scattering limits the applicability of the RE model to modulation bandwidths lower than the inverse of the scattering rate. As our predictions for the modulation bandwidth are consistently below 100 GHz, we can conclude that we are well within the applicability range of the model. However, it should be mentioned that for high power levels the effect of nonlinear gain, mediated by a finite scattering time, may further damp the modulation response.

The modulation bandwidth is defined as the frequency for which $h(\omega)$ has decreased by 3 dB. The modulation response for device A, calculated from the microscopic model, is shown in Fig. 4. Up to $P = 0.03/\text{ps}$, the resulting 3-dB frequency increases with pump rate, while for higher pump rates the 3-dB frequency is reduced again.

The dependence of the 3-dB frequency on the pump rate is shown in Fig. 5, where results for both the microscopic and the RE model are shown. It should be noted that for intermediate pump rates the agreement between the microscopic model and rate equation approach is less satisfactory than for the

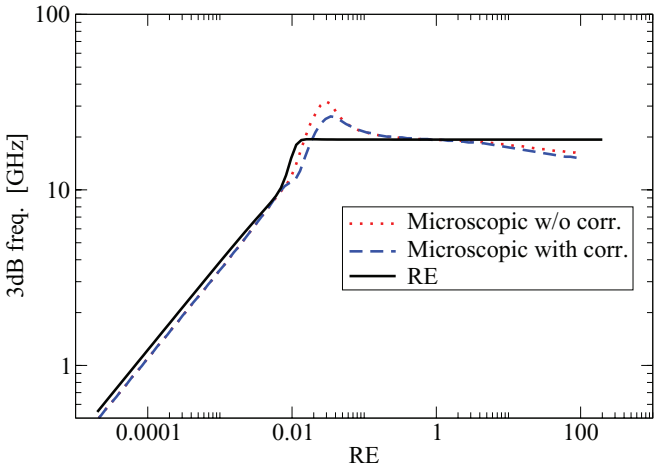

FIG. 5. (Color online) 3-dB frequency as a function of pump rate for device A as obtained from the RE model (solid black line) and the microscopic model including (blue dashed line) and neglecting (red dotted line) carrier-photon correlations.

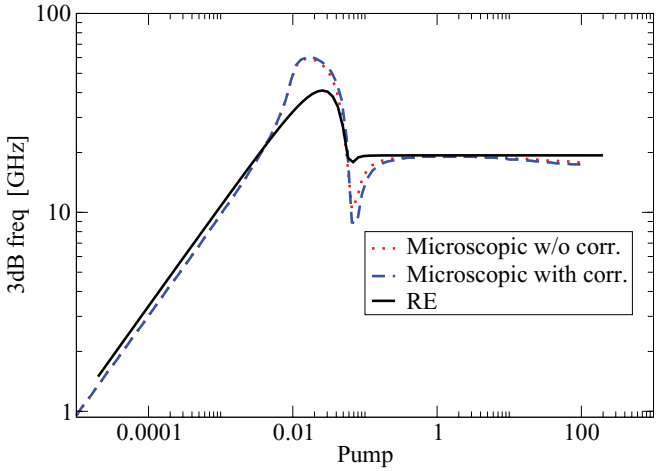

FIG. 6. (Color online) 3-dB frequency as a function of pump rate for device B as obtained from the RE model (solid black line) and the microscopic model including (blue dashed line) and neglecting (red dotted line) carrier-photon correlations.

steady-state results. This is caused by non-Markovian effects [cf. Eqs. (1)–(4)] and the additional influence of carrier-photon correlations, which are not included in an RE formalism. The slight lowering of the modulation response at extremely high pump rates in the microscopic model stems from the saturation effects in the input-output characteristics.

The general fact that the modulation response can be lowered at higher output intensities has been predicted for nanolaser devices also as a function of scattering[33] rates, and is caused by a critical damping effect. In other words, for high pump or scattering rates the relaxation oscillations become overdamped, leading to a slower time recovery in the pulse response and hence to a reduced modulation bandwidth.

Figure 6 shows the 3-dB frequency as a function of pump rate for device B. Again, the conclusions drawn from the two models are similar, though it should be noted that the influence of non-Markovian and correlation effects in the laser transition regime is stronger than for device A. Moreover, the reduction of the 3-dB frequency with pump rate is also visible in the RE model.

The detailed shape of the 3-dB versus pump curve can be understood by analytical expressions that are derived for the microscopic model by means of a small-signal analysis in Appendix B. For pump powers sufficiently above threshold, this procedure yields simple analytical expressions. The 3-dB frequency is dominated by stimulated emission and is only limited by the photon escape rate, i.e., $f_{3\text{dB}} = 2\kappa/(2\pi\hbar)$. Below threshold, spontaneous emission dominates and R_b is the largest loss term, giving 3-dB frequencies that can become larger than the above threshold result. The maximum 3-dB frequency is found below threshold at

$$f_{s,\max} = \frac{1}{2}\frac{1+\frac{2}{\hbar}\frac{\tau}{\hbar}\frac{\kappa+\gamma}{N_{\text{QD}}}}{1+\sqrt{\frac{\kappa}{\kappa+\gamma}\frac{\beta}{1-\beta}}}, \tag{20}$$

which is below threshold if $\frac{\delta}{\alpha N_{\text{QD}}} < (\frac{2\kappa}{\hbar})^2$ as detailed in Appendix B, i.e., independently of the Purcell enhancement. The excellent agreement between our two models suggests that

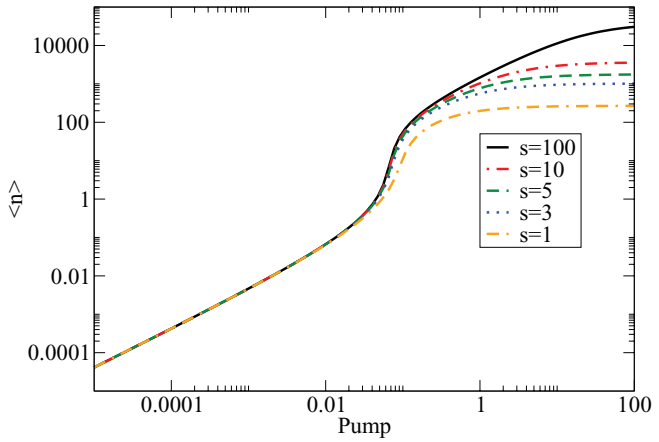

FIG. 7. (Color online) Input-output characteristics for various scattering rates $s^e = s^h = s$ in [1/ps] for device B, calculated using the microscopic model.

quantitative predictions about QD nanolasers can be obtained using the simpler RE model.

C. Influence of carrier scattering

In this section we investigate the influence of carrier scattering on the laser properties. In the rate equation presented here, carrier scattering is assumed to be instantaneous, as Fermi functions are assumed for the carrier distributions. In the microscopic model, carrier scattering is included via a phenomenological parameter, whose influence on the input-output characteristics is presented in Fig. 7. We clearly see a reduction in output power with decreasing scattering rate. This is intuitively expected, as the carrier scattering effectively acts as a pump rate for the laser levels. It should be noted that the $s = 100$ case is not physically realizable but is chosen for the comparison to the REs. As already mentioned, the generalization of the RE model to a more realistic scattering model can be easily performed, only at the cost of an increase in numerical demand. We refrained in this work from doing so, to clearly show the comparison between the two parts regarding the *optical* part of the theory. The scattering-rate-dependent

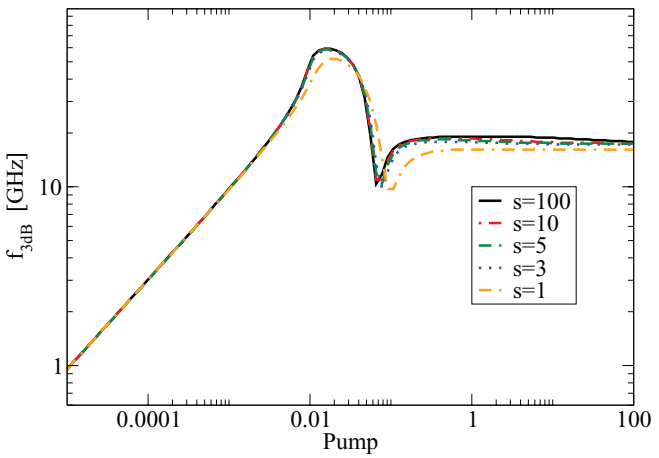

FIG. 8. (Color online) 3-dB frequency as a function of pump rate for various scattering rates $s^e = s^h = s$ in [1/ps] for device B, calculated using the microscopic model.

results for the 3-dB frequency are shown in Fig. 8. The modulation response is much less influenced by the carrier scattering than the input-ouput behavior for the parameters investigated here. This behavior stems from the fact that in this case we are in a parameter regime, where the reduction of the modulation bandwidth with scattering rate takes place at very low scattering rates. For the higher rates investigated here, the 3-dB versus scattering rate curve becomes flat. For a detailed discussion of the reduction of modulation bandwidth with carrier scattering we refer to Ref. 33.

IV. CONCLUSION

In conclusion, we have developed a rate equation model for quantum dot nanolasers that incorporates details of the optical and electronic density of states and treats Purcell enhancement of spontaneous and stimulated emission on an equal footing. The predictions of the rate equation model were compared to simulations based on microscopic laser theory, which is proven to compare well to experimental data, and very good agreement was found both for the input-output characteristics and the modulation response. The derived model is well suited for implementation into large-scale device simulations. The range of validity for these rate equations has been discussed and possible improvements highlighted.

ACKNOWLEDGMENTS

We acknowledge fruitful discussions with Bjarne Tromborg. M.L. acknowledges financial support from the Danish Research Council for Technology and Production and from the "Young Elite Researcher Award" initiative by the Danish Council for Independent Research. T.S., N.G., and J.M. acknowledge support from the Villum Kann Rasmussen Center "NATEC."

APPENDIX A: DERIVATION OF THE RATE EQUATIONS

The Einstein density rate equations for the spontaneous emission $R_{sp,21}$, the stimulated emission R_{21}, and the stimulated absorption R_{12} at the frequency ν_{21} are[34]

$$R_{sp,21} = \rho_o(\nu_{21}) h\nu_{21} B_{21} N_2, \tag{A1a}$$

$$R_{21} = W(\nu_{21}) B_{21} N_2, \tag{A1b}$$

$$R_{12} = W(\nu_{21}) B_{21} N_1, \tag{A1c}$$

where N_1 and N_2 are the state pair population densities available for upwards and downwards transitions, respectively, and ρ_o is the optical DOS. For a lasing device, the spectral energy density $W(\nu_{21})$ is usually[34] given as

$$W(\nu_{21}) = h\nu_{21} N_p \delta(\nu_c - \nu_{21}), \tag{A2}$$

and B_{21} is defined by

$$B_{21} = \frac{1}{2\hbar^2 n n_g \varepsilon_0} |\mathbf{d}|^2, \tag{A3}$$

where n_g is the group index and $|\mathbf{d}|^2$ is the dipole moment. Insertion of (A3) into (A1a) gives

$$R_{sp,21} = \frac{2\pi}{\hbar^2} \frac{\hbar\omega_{21}}{2 n n_g \varepsilon_0} |\mathbf{d}|^2 \rho_0(\omega_{21}) N_2, \tag{A4}$$

where the additional factor of 2π is due to the replacement of $\rho_o(\nu_{21})$ with $\rho_o(\omega_{21})$. In the expressions (A2) and (A4) the dependence of the spontaneous emission rate on the spatial position of the emitter in the optical environment is absent. This is strictly valid only in the case of a homogenous optical medium where the DOS is uniform in space.

A suitable generalization of (A) for an inhomogeneous optical environment at the frequency ω_{21} should involve the local density of states (LDOS), which by definition is

$$\rho_L(\hat{\mathbf{d}},\mathbf{r},\omega_{21}) = \int |\hat{\mathbf{d}}\cdot\mathbf{E}_\alpha(\mathbf{r})|^2\delta(\omega_{21}-\omega_\alpha)d\alpha. \tag{A5}$$

Here, $\hat{\mathbf{d}} = \mathbf{d}/|\mathbf{d}|$ is the dipole orientation and α is an index labeling all optical modes $\mathbf{E}_\alpha$ normalized according to

$$\int \varepsilon_r(\mathbf{r})\mathbf{E}^*_\alpha(\mathbf{r})\cdot\mathbf{E}_{\alpha'}(\mathbf{r})d\mathbf{r} = \delta(\alpha-\alpha'), \tag{A6}$$

where $\epsilon_r = n^2$ is the dielectric constant.

It is practical to split the full mode index $\alpha = (\alpha_\perp,\beta)$ into a longitudinal part β and a lateral part $\alpha_\perp$ containing the remaining indices. The mode can also be specified using the frequency instead of β as $\alpha = (\alpha_\perp,\omega)$.

Labeling the cavity mode $\alpha_{\perp,c}$, we now define separate contributions from the cavity ρ_c and the background ρ_b to the total LDOS as

$$\rho_c(\hat{\mathbf{d}},\mathbf{r},\omega_{21}) = \int |\hat{\mathbf{d}}\cdot\mathbf{E}_{\alpha_{\perp,c}}(\mathbf{r})|^2\delta(\omega_{21}-\omega_{\alpha_{\perp,c},\beta})d\beta. \tag{A7}$$

$$\rho_b(\hat{\mathbf{d}},\mathbf{r},\omega_{21}) = \int_{\alpha_\perp\neq\alpha_{\perp,c}} |\hat{\mathbf{d}}\cdot\mathbf{E}_\alpha(\mathbf{r})|^2\delta(\omega_{21}-\omega_\alpha)d\alpha_\perp d\beta, \tag{A8}$$

such that $\rho_L = \rho_c + \rho_b$.

Our generalization is now given by

$$r_{sp,21} = \int \rho_L(\hat{\mathbf{d}},\mathbf{r},\omega_{21})\hbar\omega_{21}B_{21}N_2 d\mathbf{r}, \tag{A9a}$$

$$r_{21} = \int W(\hat{\mathbf{d}},\mathbf{r},\omega_{21})B_{21}N_2 d\mathbf{r}, \tag{A9b}$$

$$r_{12} = \int W(\hat{\mathbf{d}},\mathbf{r},\omega_{21})B_{21}N_1 d\mathbf{r}, \tag{A9c}$$

with

$$W(\hat{\mathbf{d}},\mathbf{r},\omega_{21}) = \int W(\hat{\mathbf{d}},\mathbf{r},\omega_{21},\alpha_\perp)d\alpha_\perp, \tag{A10}$$

$$B_{21} = \frac{\pi}{\hbar^2\varepsilon_0}|\mathbf{d}|^2. \tag{A11}$$

The integration over volume is carried out in (A9) such that the dimension of the rates is $[s^{-1}]$. Often, the photon density is considered but this is only practical if the optical field distribution can be approximated to a constant. If not, the photon number is more suitable, and the spatial photon distribution is then described correctly by the electromagnetic field intensity.

In (A9a), the spatial dependence of the SE rate on the optical environment is taken into account using the LDOS $\rho_L(\hat{\mathbf{d}},\mathbf{r},\omega_{21})$. Accordingly, we have introduced the position and dipole-orientation-dependent spectral energy density $W(\hat{\mathbf{d}},\mathbf{r},\omega_{21})$ in the expressions (A9b)–(A9c) for the stimulated emission and absorption. It is given as an integration over an $\alpha_\perp$-dependent part $W(\hat{\mathbf{d}},\mathbf{r},\omega_{21},\alpha_\perp)$. The energy density in (A2) depends only on frequency and contains no spatial or modal dependence. To implement these, a $\alpha_\perp$-dependent occupation function $f_O(\alpha_\perp)$ should be considered, and we should use

$$W(\hat{\mathbf{d}},\mathbf{r},\omega_{21},\alpha_\perp) = f_O(\alpha_\perp)\hbar\omega_{21}\int |\hat{\mathbf{d}}\cdot\mathbf{E}_{\alpha_\perp,\beta}(r)|^2 \times \delta(\omega_{21}-\omega_{\alpha_\perp,\beta})d\beta, \tag{A12}$$

for the spectral energy density. (A12) is the direct extension of (A2) now including spatial dependence and mode-dependent occupation. If every mode is occupied by exactly one photon, $f_O(\alpha_\perp) = 1$, and the integral (A12) becomes simply proportional to the standard expression for the LDOS (A5). On the other hand, if only one lateral mode $\alpha_{\perp,c}$ is predominantly excited, as is the case for a nanolaser cavity, we have

$$f_O(\alpha_\perp) = n_p\delta(\alpha_{\perp,c}-\alpha_\perp), \tag{A13}$$

and the energy density becomes

$$W(\hat{\mathbf{d}},\mathbf{r},\omega_{21}) = n_p\hbar\omega_{21}\int |\hat{\mathbf{d}}\cdot\mathbf{E}_{\alpha_{\perp,c},\beta}(\mathbf{r})|^2\delta(\omega_{21}-\omega_{\alpha_{\perp,c},\beta})d\beta, \tag{A14}$$

where n_p is the number of photons in the mode $\alpha_{\perp,c}$. Equation (A14) corresponds to the one-dimensional case where no lateral mode index $\alpha_{\perp,c}$ is necessary, and we will skip the index $\alpha_{\perp,c}$ in the following. In this case the relation between the spectral energy density and the LDOS is simply

$$W(\hat{\mathbf{d}},\mathbf{r},\omega_{21}) = n_p\hbar\omega_{21}\rho_c(\hat{\mathbf{d}},\mathbf{r},\omega_{21}). \tag{A15}$$

The differential total stimulated emission rate $dr_{st} = dr_{21} - dr_{12}$ at the frequency ω_{21} per unit volume from the differential population densities dN_1 and dN_2 are

$$dr_{st}(\omega_{21}) = \int W(\hat{\mathbf{d}},\mathbf{r},\omega_{21})B_{21}(dN_2-dN_1) \times L(E_{21}-\hbar\omega')d\mathbf{r}\hbar d\omega', \tag{A16}$$

where the line-shape function $L(E)$ is included and $E_{21} = \hbar\omega_{21}$. The infinitesimal contributions of the number of state pairs for the upwards and downwards transitions is related to the electronic DOS $\rho_r(\mathbf{r},E)$ by

$$dN_2 = f_2(1-f_1)\rho_r(\mathbf{r},E_{21})dE_{21}, \tag{A17a}$$

$$dN_1 = f_1(1-f_2)\rho_r(\mathbf{r},E_{21})dE_{21}, \tag{A17b}$$

where f_i is the Fermi level and ρ_r is the reduced electronic DOS. Inserting (A17) into (A16) and integrating over all energies E_{21} we obtain the total stimulated emission rate given by

$$r_{st} = n_p\int \rho_c(\hat{\mathbf{d}},\mathbf{r},\omega')\hbar\omega' B_{21}\rho_r(\mathbf{r},E_{21}) \times (f_2-f_1)L(E_{21}-\hbar\omega')d\mathbf{r}dE_{21}\hbar d\omega'. \tag{A18}$$

The expression (A18) shows that the stimulated emission rate is proportional to the number of photons n_p in the cavity as expected, but it is also proportional to the cavity contribution to the LDOS at the position of the dipole emitter. Using a similar derivation, we obtain the spontaneous

emission rate into the cavity:

$$r_c = \int \rho_c(\hat{\mathbf{d}},\mathbf{r},\omega')\hbar\omega' B_{21}\rho_r(\mathbf{r},E_{21}) \times f_2(1-f_1)L(E_{21}-\hbar\omega')d\mathbf{r}dE_{21}\hbar d\omega', \quad \text{(A19)}$$

and the corresponding expression for the background r_b is obtained by replacing ρ_c with ρ_b.

The rate equation for the photon density including spontaneous and stimulated emission and a cavity loss characterized by $\tau_p^{-1} = \delta\omega_c = \omega_c/Q$ is given by

$$\frac{d}{dt}n_p = r_c + r_{st} - \frac{n_p}{\tau_p}. \quad \text{(A20)}$$

We will be using the generalized emission rates (A9) where the position-dependent LDOS is included. Using (A18) and (A19), we can express the rate equation (A20) as

$$\frac{d}{dt}n_p = \int \rho_c(\hat{\mathbf{d}},\mathbf{r},\omega')\hbar\omega' B_{21}(f_2(1-f_1)+n_p(f_2-f_1)) \times \rho_r(\mathbf{r},\hbar\omega')L(E_{21}-\hbar\omega')d\mathbf{r}dE_{21}\hbar d\omega' - \frac{n_p}{\tau_p}, \quad \text{(A21)}$$

and from this equation it is apparent that Purcell enhancement affects both spontaneous and stimulated emission. Equation (A21) is our generalized rate equation for the photon number in the cavity taking into account possible Purcell enhancement of both the spontaneous and the stimulated emission.

For $\omega' \approx \omega_c$ close to the resonance, the cavity contribution $\rho_c(\hat{\mathbf{d}},\mathbf{r},\omega')$ given in (A7) can be related to an antinode $\mathbf{r}_0$ at the cavity frequency ω_c as

$$\rho_c(\hat{\mathbf{d}},\mathbf{r},\omega') = \rho_c(\hat{\mathbf{d}}_0,\mathbf{r}_0,\omega_c)\frac{(\delta\omega_c)^2}{(\delta\omega_c)^2+4(\omega'-\omega_c)^2}\frac{|\hat{\mathbf{d}}\cdot\mathbf{E}(\mathbf{r})|^2}{|\hat{\mathbf{d}}_0\cdot\mathbf{E}(\mathbf{r}_0)|^2}. \quad \text{(A22)}$$

In the following, we for simplicity assume a dipole orientation $\hat{\mathbf{d}}$ aligned with the electric field. The cavity contribution ρ_c at an antinode $\mathbf{r}_0$ at the cavity frequency ω_c is given by

$$\rho_c(\mathbf{r}_0,\omega_c) = \frac{2Q}{\varepsilon_r V\pi\omega_c}, \quad \text{(A23)}$$

where Q is the quality factor of the cavity and V its mode volume defined by

$$V \equiv \frac{\int \epsilon_r(\mathbf{r})|\mathbf{E}(\mathbf{r})|^2 d\mathbf{r}}{\epsilon_r(\mathbf{r}_0)|\mathbf{E}(\mathbf{r}_0)|^2}. \quad \text{(A24)}$$

When integrated over all space, this integral diverges and instead a generalized mode volume[35] should be used. However, in high-Q cavities one can usually limit the integration to the geometry with negligible error.

Inserting (A23) into (A21) we obtain

$$\frac{d}{dt}n_p = \int \frac{2Q\hbar\omega' B_{21}}{\varepsilon_r V\pi\omega_c}\frac{(\delta\omega_c)^2}{(\delta\omega_c)^2+4(\omega'-\omega_c)^2} \times\frac{|\mathbf{E}(\mathbf{r})|^2}{|\mathbf{E}(\mathbf{r}_0)|^2}(f_2(1-f_1)+n_p(f_2-f_1)) \times\rho_r(\mathbf{r},E_{21})L(E_{21}-\hbar\omega')d\mathbf{r}dE_{21}\hbar d\omega' - \frac{n_p}{\tau_p}. \quad \text{(A25)}$$

To take into account the spatial dependence of the electric field profile, we can introduce the effective dielectric constant ϵ_{eff} and the confinement factor Γ[36] given by

$$\epsilon_{\text{eff}} \equiv \frac{\int \epsilon_r(\mathbf{r})|\mathbf{E}(\mathbf{r})|^2 d\mathbf{r}}{\int |\mathbf{E}(\mathbf{r})|^2 d\mathbf{r}}, \quad \text{(A26)}$$

$$\Gamma \equiv \frac{\int_{V_a}|\mathbf{E}(\mathbf{r})|^2 d\mathbf{r}}{\int |\mathbf{E}(\mathbf{r})|^2 d\mathbf{r}} = \frac{\epsilon_{\text{eff}}\int_{V_a}|\mathbf{E}(\mathbf{r})|^2 d\mathbf{r}}{V\epsilon_r(\mathbf{r}_0)|\mathbf{E}(\mathbf{r}_0)|^2}. \quad \text{(A27)}$$

We then carry out the spatial integration in (A25) and obtain

$$\frac{d}{dt}n_p = \int \frac{2Q\Gamma\hbar\omega' B_{21}}{\varepsilon_{\text{eff}}\pi\omega_c}\frac{(\delta\omega_c)^2}{(\delta\omega_c)^2+4(\omega'-\omega_c)^2} \times(f_2(1-f_1)+n_p(f_2-f_1))\rho_r(E_{21}) \times L(E_{21}-\hbar\omega')dE_{21}\hbar d\omega' - \frac{n_p}{\tau_p}. \quad \text{(A28)}$$

In this rate equations model the spontaneous emission rate is computed directly, and there is no need for the introduction of a phenomenological β factor. However, if evaluation of β is required, we can compute it as

$$\beta = \frac{r_c}{r_c + r_b}. \quad \text{(A29)}$$

APPENDIX B: ANALYTICAL EXPRESSIONS FOR THE MODULATION RESPONSE

Approximate analytical expressions can be derived for special pumping regimes using a simplified version of the CEM. The simplifications consist of the assumptions $f_p = f_p^h$ and $f_s = f_s^h$, neglecting the higher order correlations in Eq. (4) and replacing the CEM pumping term $2s\,(1-f_s)\,f_p$ by P_p^{eff}, effectively neglecting Pauli blocking of the pump contribution. With these modifications, the steady-state photon assisted polarization can be written after adiabatical elimination as

$$\langle b^\dagger v^\dagger c\rangle = \frac{1}{\kappa+\gamma}\left(f_s^2 + (2f_s-1)n_p\right). \quad \text{(B1)}$$

This results in a simplified version of (1) and (2) that can be written in a form that is similar to the LREs,

$$\dot{f}_s = P_p^{\text{eff}} - (\alpha+\delta)\,f_s^2 - \alpha\,(2f_s-1)\,n_p, \quad \text{(B2)}$$

$$\dot{n_p} = \alpha N_{QD}\left(f_s^2 + (2f_s-1)n_p\right) - \frac{2\kappa}{\hbar}n_p, \quad \text{(B3)}$$

where

$$\alpha = \frac{F}{\tau}\frac{\kappa}{\kappa+\gamma}, \quad \text{(B4)}$$

$$\delta = \frac{F}{\tau}\left(\frac{1}{\beta}-1\right). \quad \text{(B5)}$$

Linearizing the equations, the matrix elements can be written as

$$\gamma_{ff} = 2\,(\alpha+\delta)\,f_s + 2\alpha n_p, \quad \text{(B6)}$$

$$\gamma_{fn} = \alpha\,(2f_s-1)\,, \quad \text{(B7)}$$

$$\gamma_{nf} = 2\alpha N_{QD}(f_s+n_p), \quad \text{(B8)}$$

$$\gamma_{nn} = \frac{2\kappa}{\hbar} - \alpha N_{QD}\,(2f_s-1)\,. \quad \text{(B9)}$$

The 3-dB frequency is calculated as

$$\omega_R^2 = \gamma_{ff}\gamma_{nn} + \gamma_{fn}\gamma_{nf}, \tag{B10}$$

$$\gamma_R = \gamma_{ff} + \gamma_{nn}, \tag{B11}$$

$$f_{3\mathrm{dB}} = \frac{1}{2\pi}\sqrt{\omega_R^2 - \frac{\gamma_R^2}{2} + \sqrt{\left(\omega_R^2 - \frac{\gamma_R^2}{2}\right)^2 + \omega_R^4}}. \tag{B12}$$

It turns out that in most cases $\gamma_R \gg \omega_R$ and we can use the approximation,

$$f_{3\mathrm{dB}} \approx \frac{1}{2\pi}\frac{\omega_R^2}{\gamma_R} = \frac{1}{2\pi}\frac{\gamma_{ff}\gamma_{nn} + \gamma_{fn}\gamma_{nf}}{\gamma_{ff} + \gamma_{nn}}. \tag{B13}$$

Above threshold, we have $n_p \gg f_s$ which allows for the following approximations:

$$\gamma_{ff} \approx 2\alpha n_p, \tag{B14}$$

$$\gamma_{nf} \approx 2\alpha N_{QD} n_p, \tag{B15}$$

$$\gamma_{nn} \approx 0. \tag{B16}$$

The last approximation is clear from the above threshold steady-state equation for n_p, i.e.,

$$\dot{n}_p = \alpha N_{\mathrm{QD}}\left(f_s^2 + (2f_s - 1)\, n_p\right) - \frac{2\kappa}{\hbar} n_p = 0,$$

$$0 \approx \alpha N_{\mathrm{QD}}\,(2f_s - 1) - \frac{2\kappa}{\hbar}. \tag{B17}$$

Thus we have

$$f_{3\mathrm{dB}} \approx \frac{1}{2\pi}\frac{\gamma_{fn}\gamma_{nf}}{\gamma_{ff}} = \frac{1}{2\pi}\frac{\alpha\,(2f_s - 1)\,2\alpha N_{\mathrm{QD}} n_p}{2\alpha n_p}$$

$$= \frac{1}{2\pi}\alpha N_{\mathrm{QD}}\,(2f_s - 1) = \frac{1}{2\pi}\frac{2\kappa}{\hbar}. \tag{B18}$$

This corresponds exactly to the observed above threshold behavior when Pauli blocking is neglected.

Below threshold it is found that $\gamma_{ff}\gamma_{nn} \gg \gamma_{fn}\gamma_{nf}$ so that we can write

$$f_{3\mathrm{dB}} \approx \frac{1}{2\pi}\frac{\gamma_{ff}\gamma_{nn}}{\gamma_{ff} + \gamma_{nn}} = \frac{1}{2\pi}\left[\frac{1}{\gamma_{ff}} + \frac{1}{\gamma_{nn}}\right]^{-1}. \tag{B19}$$

Equation (B19) is controlled by the matrix elements γ_{ff} and γ_{nn}, the latter of which can be rewritten as $\gamma_{nn} = \frac{\alpha N_{\mathrm{QD}} f_s^2}{n_p}$. For below threshold operation where the photon density is low, γ_{nn} will be larger than γ_{ff} and Eq. (B19) therefore simplifies to

$$f_{3\mathrm{dB}} \approx \frac{1}{2\pi}\gamma_{ff} = \frac{1}{2\pi}2\,(\alpha + \delta)\, f_s + 2\alpha n_p$$

$$\approx \frac{1}{2\pi}2\delta f_s, \tag{B20}$$

where the last approximation is valid for $\alpha \ll \delta$, which is the case for low β factors. From Eq. (B20) we can see that for devices with sufficiently low β the below threshold behavior is controlled by the spontaneous emission into the background. This is reflected in the difference between the 3-dB frequency for the device with $\beta = 0.3$ and the device with $\beta = 0.1$, where $f_{3\mathrm{dB}}$ is significantly higher for the low β device. For sufficiently low β and high F_p, the below threshold 3-dB frequency can even surpass the cavity photon loss which usually determines the upper limit of the bandwidth. This gives rise to the maximum in Fig. 5 which can be found from $\frac{df_s}{df_{3\mathrm{dB}}} = 0$,

$$f_{s,\max} = \frac{1}{2}\frac{1 + \frac{2\kappa}{\hbar\alpha N_{\mathrm{QD}}}}{1 + \sqrt{\frac{\delta}{\alpha N_{\mathrm{QD}}}}}. \tag{B21}$$

The maximum $f_{3\mathrm{dB}}$ can be found by inserting Eq. (B21) back into Eq. (B19), but it does not result in a simple expression.

Equations (B19) and (B18) closely reproduce the behavior of the 3-dB frequency sufficiently far away from threshold. The dip in the 3-dB frequency at transparency can also be approximately described by assuming $\gamma_{ff} \gg \gamma_{nn}$, which is fulfilled close to threshold. Then,

$$f_{3\mathrm{dB}} \approx \frac{1}{2\pi}\left(\gamma_{nn} + \frac{\gamma_{fn}\gamma_{nf}}{\gamma_{ff}}\right), \tag{B22}$$

where we have from the steady-state equations and Eqs. (B6)–(B9):

$$\gamma_{nn} = \frac{2\kappa}{\hbar} - \alpha N_{\mathrm{QD}}(2f_s - 1) = \alpha N_{\mathrm{QD}}\frac{f_s^2}{n_p},$$

$$\frac{\gamma_{fn}\gamma_{nf}}{\gamma_{ff}} = \frac{2\alpha^2 N_{\mathrm{QD}}(2f_s - 1)(f_s + n_p)}{2(\alpha + \delta) f_s + 2\alpha n_p} = \frac{\frac{2\kappa}{\hbar} - \alpha N_{\mathrm{QD}}\frac{f_s^2}{n_p}}{1 + \frac{\delta}{\alpha}\frac{f_s}{f_s + n_p}}. \tag{B23}$$

Thus, the 3-dB bandwidth becomes

$$f_{3\mathrm{dB}} \approx \frac{1}{2\pi}\frac{\frac{2\kappa}{\hbar} + \alpha N_{QD}\frac{f_s^2}{n}\epsilon}{1 + \epsilon}, \tag{B24}$$

where $\epsilon = \frac{\delta}{\alpha}\frac{f_s}{f_s + n_p} = \frac{d_{f_s} R_b}{d_{f_s}(R_c + R_s)}$. From this we see that above threshold, where $n_p \gg f_s$, $\epsilon \approx 0$, so that $f_{3\mathrm{dB}} = \frac{1}{2\pi}\frac{2\kappa}{\hbar}$. Below threshold $\epsilon \approx \frac{\delta}{\alpha}$ and therefore $f_{3\mathrm{dB}} = \frac{1}{2\pi}\frac{\alpha\delta}{\alpha+\delta} N_{\mathrm{QD}}\frac{f_s^2}{n_p}$, so that $f_{3\mathrm{dB}}$ first increases and then decreases as n_p becomes comparable to f_s^2. For $n_p \gg 1$, the above threshold expression for the bandwidth is recovered.

*Present address: Bremen Center for Computational Materials Science, University of Bremen, Germany; mlorke@itp.uni-bremen.de.

[1] Y. Akahane, T. Asano, B.-S. Song, and S. Noda, Nature (London) **425**, 944 (2003).

[2] S. Noda, M. Fujita, and T. Asano, Nat. Photon. **1**, 449 (2007).

[3] M. Bayer, T. L. Reinecke, F. Weidner, A. Larionov, A. McDonald, and A. Forchel, Phys. Rev. Lett. **86**, 3168 (2001).

[4] J. P. Reithmaier, G. Sek, A. Löffler, C. Hofmann, S. Kuhn, S. Reitzenstein, L. V. Keldysh, V. D. Kulakovskii, T. L. Reinecke, and A. Forchel, Nature (London) **432**, 197 (2004).

[5]T. Yoshie, A. Scherer, J. Hendrickson, G. Khitrova, H. M. Gibbs, G. Rupper, C. Ell, O. B. Shchekin, and D. G. Deppe, Nature (London) **432**, 200 (2004).
[6]M. Nishioka, R. Schur, M. Kitamura, H. Watabe, and Y. Arakawa, Physica B **227**, 404 (1996).
[7]H. Saito, K. Nishi, I. Ogura, S. Sugou, and Y. Sugimoto, Appl. Phys. Lett. **69**, 3140 (1996).
[8]K. Vahala, Nature (London) **424**, 839 (2003).
[9]P. Lodahl, A. Floris van Driel, I. S. Nikolaev, A. Irman, K. Overgaag, D. Vanmaekelbergh, and W. L. Vos, Nature (London) **430**, 654 (2004).
[10]B. Ellis, I. Fushman, D. Englund, B. Zhang, Y. Yamamoto, and J. Vučković, Appl. Phys. Lett. **90**, 151102 (2007).
[11]D. Englund, H. Altug, and J. Vučković, J. Appl. Phys. **105**, 093110 (2009).
[12]E. K. Lau, A. Lakhani, R. S. Tucker, and M. C. Wu, Opt. Express **17**, 7790 (2009).
[13]M. Lorke, T. R. Nielsen, and J. Mørk, Appl. Phys. Lett. **99**, 151110 (2011).
[14]T. Suhr, N. Gregersen, K. Yvind, and J. Mørk, Opt. Express **18**, 11230 (2010).
[15]T. Suhr, N. Gregersen, M. Lorke, and J. Mørk, Appl. Phys. Lett. **98**, 211109 (2011).
[16]N. Gregersen, T. Suhr, M. Lorke, and J. Mørk, Appl. Phys. Lett. **100**, 131107 (2012).
[17]H. Altug, D. Englund, and J. Vučković, Nat. Phys. **2**, 484 (2006).
[18]C. Gies, J. Wiersig, M. Lorke, and F. Jahnke, Phys. Rev. A **75**, 013803 (2007).
[19]S. M. Ulrich, C. Gies, J. Wiersig, S. Reitzenstein, C. Hofmann, A. Löffler, A. Forchel, F. Jahnke, and P. Michler, Phys. Rev. Lett. **98**, 043906 (2007).
[20]M. Lermer, N. Gregersen, M. Lorke, E. Schild, P. Gold, J. Mørk, C. Schneider, A. Forchel, S. Reitzenstein, S. Höfling, and M. Kamp, Appl. Phys. Lett. **102**, 052114 (2013).
[21]J. Wiersig, C. Gies, F. Jahnke, M. Aszmann, T. Berstermann, M. Bayer, C. Kistner, S. Reitzenstein, C. Schneider, S. Hofling, A. Forchel, C. Kruse, J. Kalden, and D. Hommel, Nature (London) **460**, 245 (2009).
[22]H. Yokoyama and S. D. Brorson, J. Appl. Phys. **66**, 4801 (1989).
[23]Y. Yamamoto, S. Machida, and G. Bjork, Phys. Rev. A **44**, 657 (1991).
[24]G. Björk, Jour. Quant. Elec. **27**, 2386 (1991).
[25]A. J. Campillo, J. D. Eversole, and H.-B. Lin, Phys. Rev. Lett. **67**, 437 (1991).
[26]M. Djiango, T. Kobayashi, and W. J. Blau, Appl. Phys. Lett. **93**, 143306 (2008).
[27]T. R. Nielsen, P. Gartner, and F. Jahnke, Phys. Rev. B **69**, 235314 (2004).
[28]J. Seebeck, T. R. Nielsen, P. Gartner, and F. Jahnke, Phys. Rev. B **71**, 125327 (2005).
[29]T. Markussen, P. Kristensen, B. Tromborg, T. W. Berg, and J. Mørk, Phys. Rev. B **74**, 195342 (2006).
[30]N. Baer, C. Gies, J. Wiersig, and F. Jahnke, Eur. Phys. J. B **50**, 411 (2006).
[31]M. Lorke, T. R. Nielsen, J. Seebeck, P. Gartner, and F. Jahnke, Phys. Rev. B **73**, 085324 (2006).
[32]P. Michler, *Single Quantum Dots—Fundamentals, Applications and New Concepts* (Springer-Verlag, Berlin, 2003).
[33]M. Lorke, T. R. Nielsen, and J. Mørk, Appl. Phys. Lett. **97**, 211106 (2010).
[34]L. A. Coldren and S. W. Corzine, *Diode Lasers and Photonic Integrated Circuits* (Wiley, New York, 1995).
[35]P. T. Kristensen, C. Van Vlack, and S. Hughes, Opt. Lett. **37**, 1649 (2012).
[36]A. Mock, J. Opt. Soc. Am. B **27**, 2262 (2010).